nature nanotechnology

SUPPLEMENTARY INFORMATION

DOI: 10.1038/NNANO.2011.214

Control over topological insulator photocurrents with light polarization

J.W. McIver*, D. Hsieh*, H. Steinberg, P. Jarillo-Herrero and N. Gedik

DOI: 10.1038/NNANO.2011.214

SI I. Materials and device fabrication

Bi_2Se_3 single crystals were synthesized by melting a stochiometric mixture of Bi and Se, where excess Se was used to compensate for the Se vacancies that give rise to bulk doping [33]. Specifically, the initial mixture of Bi:Se 2:4.06 was heated in a sealed quartz tube to 850°C where it was kept for 48 hours. It was then cooled down over five days and annealed at 550°C for an additional five days. The resulting material was studied by low temperature (4K) magneto-transport and was found to be electron doped with a bulk carrier density (n) of $n \sim 2 \times 10^{17}$ cm^{-3} and a bulk carrier mobility (μ) of $\mu \sim 6000 - 8000$ cm^2/Vs. We note that the doping concentration in these materials increases due to the processing of nano-devices.

The devices were fabricated using a similar technique to that reported in [20]. An Atomic Force Microscopy (AFM) image of a typical device contacted in a two-terminal geometry is shown in Figure 1(c) of the main text. The devices were fabricated by mechanically exfoliating Bi_2Se_3 flakes to a nanometric thickness and depositing them on a SiO_2 surface. Bi_2Se_3 flakes measured in this study were 120 nm thick and typically 3.5 μm wide and 5 μm long. Suitable flakes of a smooth top surface were identified using optical and AFM imaging techniques. The flakes were contacted by evaporated electrodes (5 nm Ti, 100 nm Al) patterned using standard electron beam lithography procedures.

SI II. Photocurrent symmetry analysis in Bi_2Se_3(111)

The dominant dc current response ($\vec{j}$) to an oscillating electromagnetic field with a complex electric field component $\vec{E}(\vec{q},\omega)$ is given by [24]

$$j_\lambda(0,0) = \sigma_{\lambda\nu\eta}(\vec{q},\omega)E_\nu(\vec{q},\omega)E^*_\eta(\vec{q},\omega) \quad (1)$$

where $\sigma_{\lambda\nu\eta}(\vec{q},\omega)$ is a photocurrent conductivity tensor, the indices run through three spatial coordinates, $\vec{q}$ is the photon linear momentum, and ω is the photon frequency. Expanding the second order conductivity $\sigma_{\lambda\nu\eta}(\vec{q},\omega)$ to linear order in $\vec{q}$, we find that

$$\sigma_{\lambda\nu\eta}(\vec{q},\omega) = \sigma_{\lambda\nu\eta}(0,\omega) + \Phi_{\lambda\mu\nu\eta}(\omega)q_\mu \quad (2)$$

The first and second terms, dubbed the photogalvanic and photon drag effects respectively, differentiate between optical processes that do not and do involve the transfer of linear momentum from the incident photons to the excited electrons as a means of generating current. Because j_λ is odd under the operation of space inversion symmetry but the square of the electric field is even, $\sigma_{\lambda\nu\eta}(0,\omega)$ has non-zero components only for systems that break inversion symmetry. Therefore, in an inversion-symmetric material such as Bi_2Se_3 (space group D^5_{3d}) [15], photogalvanic effects are only allowed at the surface where the symmetry is reduced to C_{3v}. Photon drag effects, on the other hand, are described by a higher-order conductivity tensor $\Phi_{\lambda\mu\nu\eta}$ that has an even rank. Because even rank tensors may have non-zero components in inversion-symmetric systems, photon drag is permitted by symmetry to exist in the bulk of Bi_2Se_3. Because both $\sigma_{\lambda\nu\eta}(0,\omega)$ and $\Phi_{\lambda\mu\nu\eta}(\omega)$ may have off-diagonal elements, photocurrent magnitudes may differ along different crystal axes. While this analysis does not guarantee the presence of a particular photocurrent class, it serves as a useful guide for identifying potential contributions.

DOI: 10.1038/NNANO.2011.214

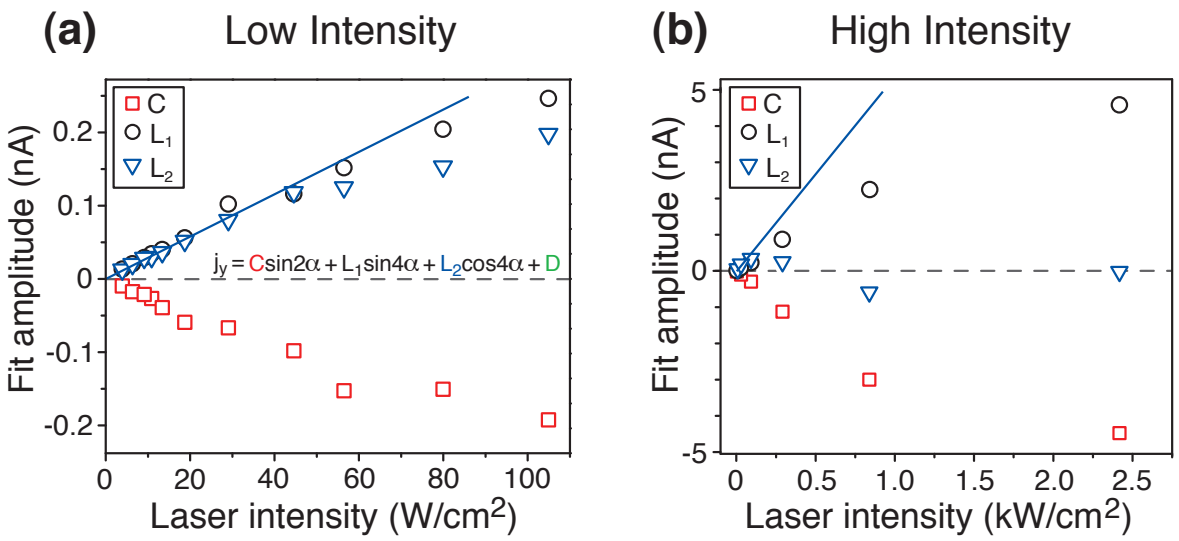

FIG. S1: Photocurrent $j_y(\alpha)$ fit amplitudes in the Fig.2(a) (main text) geometry over a broad range of laser intensities at 15 K. (a) Low intensity regime. (b) High intensity regime. The blue line is drawn to highlight the sub-linear behavior at high intensities.

SI III. Deviation from linear photocurrent response at higher laser intensities

As shown by eq. (1) in the previous section, photocurrents are expected to scale quadratically with the ac electric field of the incident light, which is to say that they scale linearly with the laser intensity. Figure 1(e) of the main text shows that $j_y(\alpha = 0)$ scales linearly with laser intensity up until around $I = 60$ W/cm^2, below which is the low intensity regime where all reported photocurrent measurements were performed. Here we show the intensity dependence of the corresponding polarization dependent fit coefficients C, L_1 and L_2 from eq.(1) of the main text over a broad range of laser intensities. Figure S1(a) shows that their amplitudes likewise begin to deviate from the expected linear scaling when intensities of greater than $I = 60$ W/cm^2 are used, and become highly sub-linear at even greater intensities [Fig.S1(b)]. These behaviors may be attributed to a combination of multi-photon absorption processes, the saturation of certain interband transitions, and a temperature increase caused by excessive laser heating. The last-mentioned is likely responsible for the sub-linearity since Fig.3(a) of the main text shows that the photocurrent amplitudes decrease as the temperature is increased. This is further evidenced by the sign reversal of L_2 in Fig.S1(b), which likewise occurs in the temperature dependence. It is therefore necessary that all photocurrent measurements on Bi_2Se_3 be performed at low laser intensities.

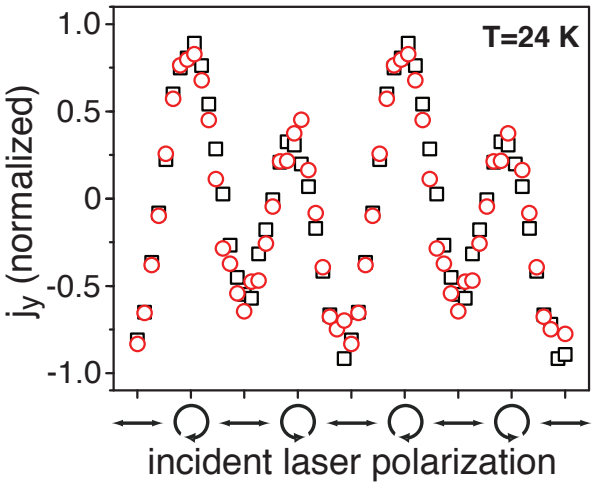

FIG. S2: Photocurrent $j_y(\alpha)$ taken with pulsed (red circles) and continuous wave (black squares) 795 nm laser light. Traces were taken in the Fig.2(a) (main text) geometry at 24 K and were normalized to account for the small laser intensity changes that accompany changing the laser emission mode, which slightly modify the current amplitude, to highlight the identical polarization dependence.

SI IV. Identical photocurrent response by continuous wave and pulsed laser excitation

While pulsed laser light is standardly used to induce polarization dependent photocurrents in quantum well structures [24], we confirmed independently that the pulsed nature of the light does not influence $j_y(\alpha)$. Fig.S2 shows that traces taken with continuous wave laser light and pulsed laser light of the same wavelength are virtually identical.

DOI: 10.1038/NNANO.2011.214

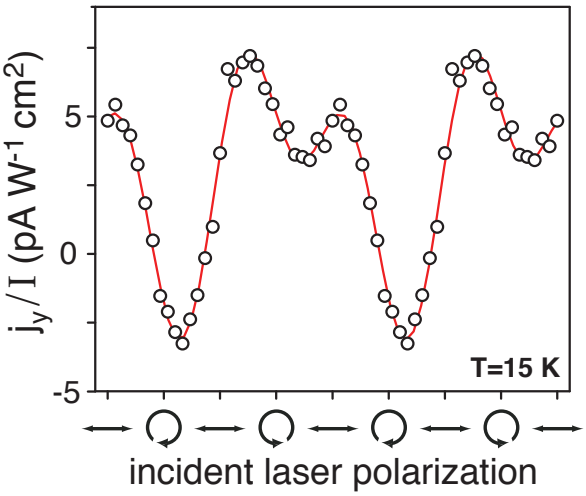

FIG. S3: Photocurrent $j_y(\alpha)/I$ measured on a different device in the Fig.2(a) (main text) geometry at 15 K.

SI V. Consistent results across multiple devices

To confirm that the photon polarization induced currents observed were consistent across multiple devices, a second device of similar dimensions was characterized [Fig.S3]. The photocurrent response $j_y(\alpha)$ of the second device proved to be qualitatively similar to the data reported in the main text. The slight differences between the signals may be due to a different crystal axes orientation relative to the contacts, which could affect the relative photocurrent magnitudes as discussed in SI II.

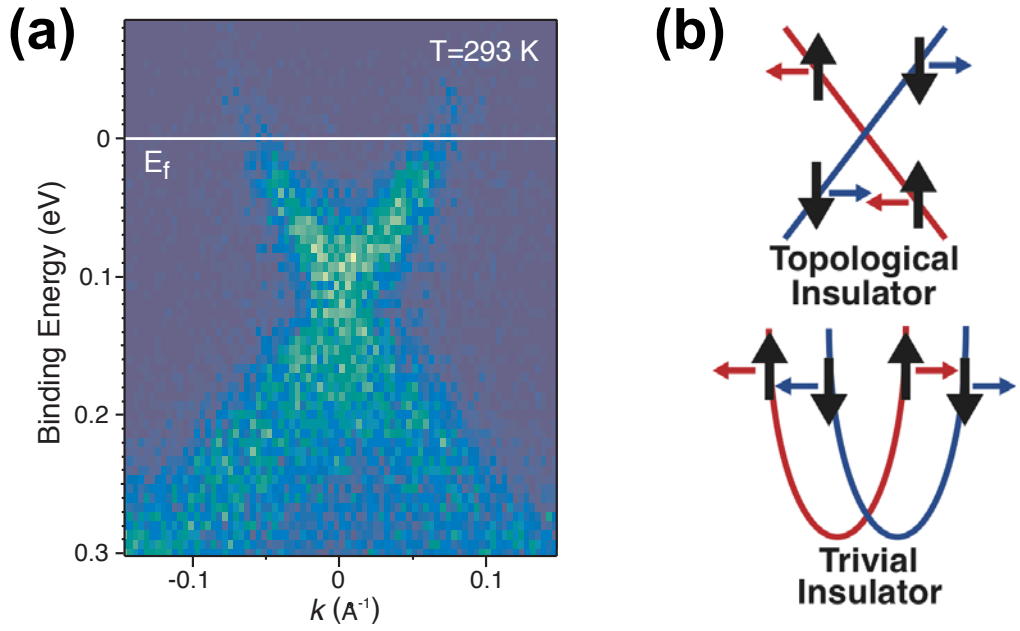

FIG. S4: (a) ARPES spectrum of the Bi_2Se_3 material used to fabricate devices revealing the absence of Rashba-split states in ultra-high vacuum. (b) Comparison of Rashba-split quantum well states and topological surface states. CPGE currents induced in Rashba-split states experience a cancellation effect that is absent in the linearly dispersing surface states.

SI VI. Ruling out alternative photocurrent mechanisms

A. Circular photogalvanic effect from Rashba-split quantum well states in the inversion layer

The circular photogalvanic effect (CPGE) has been observed from Rashba spin-split states in quantum well structures [24,25]. Similar states have been observed using ARPES in the surface inversion layer of Bi_2Se_3 samples that were intentionally surface electron doped by depositing certain gases or metals on the surface [34-36]. To check for these states, we performed ARPES measurements on our Bi_2Se_3 material [Fig.S4]. The spectrum was taken in ultrahigh vacuum and at room temperature several hours after the sample was cleaved to approximate the band-bending that occurs in air. We find no evidence of Rashba-splitting. The Fermi level is approximately 120 meV above the Dirac point. Typically, Rashba-split states do not appear until the surface Fermi level is doped to around 600 meV above the

DOI: 10.1038/NNANO.2011.214

Dirac point [34-36].

While we find no evidence of Rashba-splitting in samples cleaved in UHV, we acknowledge that the device fabrication process does electron dope our material. However, even if the doping during fabrication were sufficient to induce Rashba-splitting in the inversion layer, the CPGE contribution from these states can be expected to be small in comparison to that from the surface states. This is because in Rashba spin-split systems there are two oppositely spin-polarized Fermi surfaces so that it is possible to have electrons of the same spin propagating in opposite directions. Any currents induced by creating a net spin density, such as through CPGE, will therefore experience a cancellation effect with a net current magnitude proportional to the spin-splitting, which is only a fraction of the Fermi momentum k_f [Fig.S4(b)]. Topological surface states, on the other hand, have a single helical spin distribution, so there is no cancellation effect, with a current magnitude that is proportional to the effective spin-splitting across the Dirac cone, which is $2k_f$. For this reason, topological surface states are generally expected to have a much larger spin-density induced current than Rashba systems [14,37]. However, if the depth that the inversion layer penetrated into the bulk were very large, it is true that CPGE from these states could dominate our signal. We estimate the depth that the Rashba-split states would penetrate into the bulk if they were present in our material. We typically measure a bulk carrier density of n$\sim$5x10^{18} cm^{-3} in our exfoliated Bi_2Se_3 flakes patterned in a Hall bar device geometry. From this and the reported values for the average effective mass and dielectric constant [33] we estimate that the inversion layer thickness is only $\sim$ 2 nm using the Thomas-Fermi screening length as an approximation. This is comparable to the depth (d) that the surface states penetrate into the bulk, which is roughly $d = \hbar v_f/\Delta \sim 1$ nm, where v_f is the surface state Fermi velocity and Δ is the bulk band gap. This shows that the cumulative CPGE contribution from Rashba-split states over the entire inversion layer depth can still be expected to be small.

B. Photo-induced inverse spin Hall effect

A photo-induced inverse spin Hall effect has been observed in bulk GaAs [38,16]. In this effect, optically spin oriented electrons excited on the surface diffuse into the bulk and undergo spin-dependent scattering to generate a helicity-dependent photocurrent. This

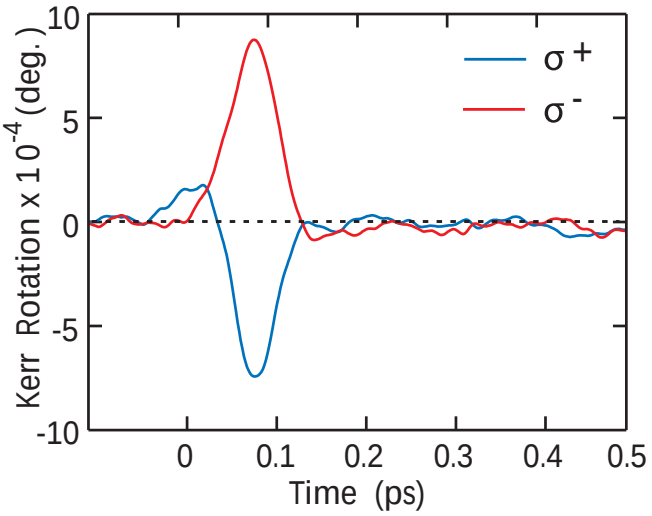

FIG. S5: Time-resolved Kerr rotation spectroscopy measurement on the same Bi_2Se_3 material used to fabricate devices. A 100 fs circularly polarized pump pulse of 795 nm laser light creates a non-equilibirum bulk state spin-polarization. The spin relaxation dynamics are probed by monitoring the Kerr rotation of a time-delayed linearly polarized probe pulse. σ^+ and σ^- represent left and right circular polarizations respectively.

effect can occur in GaAs because of the unique nature of its spin-orbit coupling. The spin-orbit coupled valance band permits the optical spin orientation of electrons excited to the conduction band by circularly polarized light. Owing to the s-orbital nature (zero spin-orbit coupling) of the conduction band, the spin-lifetime of these electrons is exceptionally long, on the order of 10-100 ns [39]. This is long enough for optically excited carriers on the surface to diffuse into the bulk while retaining their spin polarization. Spin-dependent scattering can then occur to generate a spin Hall effect current.

In materials such as Bi_2Se_3, any photo-induced spin-polarized bulk states will rapidly depolarize before significant diffusion can occur. This is because both the initial and final states are spin-orbit coupled (p-orbital nature), in contrast to GaAs, which greatly reduces the spin-lifetime of excited carriers. To show that this is the case, we performed time-resolved Kerr rotation spectroscopy measurements on the same material used to fabricate devices [Fig.S5]. A more extensive study was performed in ref. [40]. We find that the spin-polarization of optically oriented bulk carriers completely depolarizes in $\sim$ 100 fs, which is the resolution limit of our measurement. This is 5-6 orders of magnitude shorter than

DOI: 10.1038/NNANO.2011.214

the spin-lifetime in GaAs and short enough that any carrier diffusion from the surface into the bulk can be expected to have a negligible spin-polarization. Contributions from the photo-induced inverse spin Hall effect can therefore be expected to be very small in Bi_2Se_3.

Furthermore, the presence of the photocurrent L_1 that appears to be linked to the helicity-dependent current C [Fig.2 main text] cannot be accounted for by this effect.

---

[33] Analytis, J.G. *et al.* Bulk Fermi surface coexistence with Dirac surface state in Bi_2Se_3: A comparison of photoemission and Shubnikov-de Haas measurements. *Phys. Rev. B* **81**, 205407 (2010).

[34] Wray, L.A. *et al*. A topological insulator surface under strong Coulomb, magnetic and disorder perturbations. *Nature Phys.* **7**, 32-37 (2010).

[35] Bianchi, M. *et al*. Simultaneous quantization of bulk conduction and valence state through adsorption of nonmagnetic impurities on Bi_2Se_3. arXiv: 1105.3826 (2011).

[36] Wray, L.A. *et al*. Electron dynamics in topological insulator based semiconductor-metal interfaces (topological p-n interface based on Bi_2Se_3 class. arXiv: 1105.4794 (2011).

[37] Yazyev, O., Moore, J., Louie, S. Spin polarization and transport of surface states in the topological insulators Bi_2Se_3 and Bi_2Te_3 from first principles. *Phys. Rev. Lett.* **105**, 266806 (2010).

[38] Bakun, A.A. *et al*. Observation of a surface photocurrent caused by optical orientation of electrons in a semiconductor. *JETP Lett.* **35**, 196 (1984).

[39] Kikkawa, J.M. & Awschalom, D.D. Resonant spin amplification in *n*-type GaAs. *Phys. Rev. Lett.* **80**, 4313-4316 (1998).

[30] Hsieh, D. *et al.* Selective probing of photoinduced charge and spin dynamics in the bulk and surface of a topological insulator. *Phys. Rev. Lett.* **107**, 077401 (2011).